2011 IEEE/RSJ International Conference on
Intelligent Robots and Systems
September 25-30, 2011. San Francisco, CA, USA

Image-Based Magnetic Control of Paramagnetic Microparticles in Water

Jasper D. Keuning*, Jeroen de Vries†, Leon Abelmann† and Sarthak Misra*
University of Twente, The Netherlands

Abstract— **This paper describes the design of a system for controlling the position of spherical paramagnetic microparticles that have an average diameter of 100 µm. The focus of this study lies in designing and implementing a system that uses microscopic images and electromagnets. Preliminary experiments have been done to verify the feasibility of the system to track and control the position of these particles. A vibrating sample magnetometer was used to determine the magnetic moment of the particles. Finite element method simulations were used to verify the magnetic behavior of the designed setup. The system was used to position the particles within 8.4 µm of a setpoint, achieving speeds of up to 235 µm s^{-1}. We also demonstrated that the particle could follow a circular and a figure-eight path.**

I. INTRODUCTION

Minimally invasive surgery (MIS) focuses on reducing patient surgical trauma while enabling clinicians to reach deep-seated locations within the human body. Further, robotic MIS aims to benefit medicine by further reducing invasiveness of MIS, improve clinical outcomes, minimize patient trauma, and enable treatment of inoperable patients. Such robotic systems can be inserted into the body, and use natural pathways within the body, such as arteries and veins or the gastrointestinal tract, to reach their target for drug delivery or diagnosis [1]. Reducing the size of these robots will increase their potential penetration depth inside the body. The smaller size means they will be able to travel through smaller pathways to reach their target.

A significant amount of research has been done on miniaturizing robots for a variety of applications [2]. An important aspect of these robotic systems is their propulsion mechanism. When robots are scaled down, the space available to store energy for propulsion within the robot reduces. In most microrobots the energy needed to move around is provided externally. There are many different ways propulsion energy can be delivered to the robot. Within the domain of untethered microrobotic systems, a widely used method to deliver this energy, is by means of (electro)magnetic fields [3].

There are several ways magnetic fields can be utilized to control microrobotic systems. Kummer et al. [4] demonstrated a system using eight electromagnets to control a robot. They showed that this setup can position a 500 µm soft magnetic body using both open and closed loop control. Similar systems that use magnetic forces to position hard magnetic [5], soft magnetic [6], [7] and paramagnetic bodies [8] have been presented in literature. A helical-shaped robot can be propelled forward by rotating around its axis. This rotation can be achieved by periodically changing the rotation of the magnetic field at the location of the robot [9], [10].

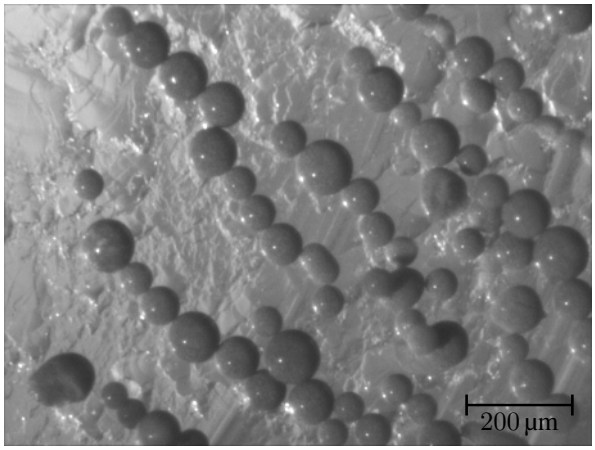

Fig. 1. The paramagnetic particles used in the experiments. The particles have diameters ranging from 60 µm to 110 µm.

The use of magnetic fields to provide energy to the robots is however extremely inefficient. Magnetic coil systems for propulsion generate alternating fields in large volumes of at least several cubic centimeters. Out of that field, only a tiny fraction of at most a cubic millimeter is used by the robot, resulting in efficiencies smaller than 1×10^{-3}. Rather than extracting energy from the field, the robots can extract energy from the liquid into which they are residing. A static magnetic field can then be used for steering only, which requires far less energy than an alternating field. Martel and Mohammadi [11] demonstrated the possibility to use magnetotactic bacteria to position microscopic structures for self-assembly purposes. The bacteria provide the propulsion whereas the magnetic field is used to guide the bacteria to the desired positions.

Alternatively, one can use catalytic motors that extract energy from their surroundings. The energy for the propulsion comes from a chemical reaction between material that is part of the robot and the fluid it is immersed in [12]–[15].

In this paper, we describe the implementation of a compact experimental setup that will be used to study the control of self-propelled microrobots. We present the design of the setup and demonstrate its capabilities by doing preliminary experiments on the closed-loop control of paramagnetic microparticles (Fig. 1). Similar setups have been designed by the previously mentioned researchers, though the results obtained from our work will serve as a foundation for future

*MIRA–Institute of Biomedical Technology and Technical Medicine
†MESA+ Institute for Nanotechnology

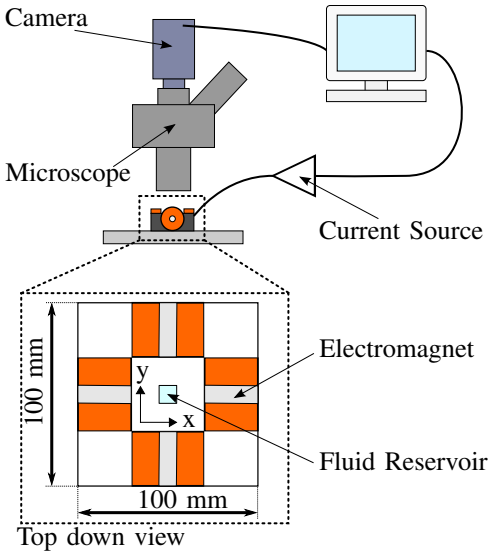

Fig. 2. The camera takes images of the particles in the reservoir using a microscope. The images are processed and control signals for the electromagnets are generated. The size of the fluid reservoir is 10 mm×10 mm.

work on self-propelled microrobots. The paper is organized as follows: Section II describes the various aspects involving the design of the setup, the tracking and the control of the paramagnetic microparticles. Section III discusses the experimental results obtained. Finally, Section IV provides conclusions and possible directions for future work.

II. EXPERIMENTAL SETUP

The proposed setup to observe and control the position of the particles under the influence of magnetic fields is shown in Fig. 2. The main components are a fluid reservoir for the paramagnetic particles and the magnets surrounding this reservoir. A Sony XCD-X710 (Sony Corporation, Tokyo, Japan) 1024×768 pixels FireWire camera is mounted on a Mitutoyo FS70 microscope unit (Mitutoyo, Kawasaki, Japan) using a Mitutoyo M Plan Apo 2× / 0.055 Objective. A control computer is used to acquire the images and track the particles, as well as to control their position by means of Proportional-Integral (PI) controllers. The input provided to the controllers is the difference between the current location, and the desired position of the particle. The output of the controllers is used to set the current through the coils.

A. General design considerations

The reservoir needs to be viewable underneath the microscope. There should be space available for the microscope objective to be positioned properly above the target. Also since the setup needs to be placed underneath the microscope, the total footprint is limited in its size. With the available microscope setup, the camera will have a field of view of 2.4 mm × 1.8 mm (2.34 µm per pixel). The size of the reservoir will be equal or larger then the field of view. The particles that are going to be controlled will be floating in the water-to-air boundary layer. Near the edges of the reservoir it is expected that due to surface tension, the surface of the liquid will form a meniscus. Increasing the size of the reservoir will reduce the magnitude of this meniscus near its center. Based on these considerations we have decided to design a setup with a footprint of 100 mm × 100 mm. The fluid reservoir will be 10 mm × 10 mm with a depth of 5 mm.

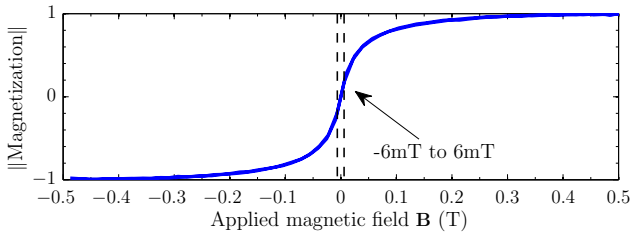

Fig. 3. Normalized mass magnetization of the paramagnetic particles.

B. Paramagnetic microparticles

We are using paramagnetic spherical microparticles, consisting of iron-oxide in a poly(lactic acid) matrix (PLA-Particles-M-redF-plain from Micromod Partikeltechnologie GmbH, Rostock-Warnemuende, Germany). These particles have an average diameter of ∼100 µm. Paramagnetic particles are preferred over ferromagnetic particles because they were readily available and because they have a more favorable magnetization curve. We assume that the only force opposing the magnetic force is the viscous drag force. The velocity of the particle in the water is therefore determined by the balance between the magnetic force and viscous drag force.

The magnetic force exerted on a paramagnetic microparticle can be calculated using the following equation [8]:

$$\mathbf{F} = \nabla(\mathbf{m} \cdot \mathbf{B}) \tag{1}$$

where $\mathbf{m}$ is the magnetic moment of the particle and $\mathbf{B}$ is the applied magnetic field. For a paramagnetic microparticle, $\mathbf{m}$ can be expressed as,

$$\mathbf{m} = \alpha_\mathrm{p} V_\mathrm{p} \mathbf{B} \tag{2}$$

where V_p is the volume of the particle. The value of α_p was determined by measuring $\mathbf{m}$ of the particles as a function of $\mathbf{B}$ in a vibrating sample magnetometer (Fig. 3). At the expected field of 6 mT, α_p can be approximated by a constant. According to the manufacturer, the saturation mass magnetization of the particle is $6.6 \times 10^{-3}\,\mathrm{A\,m^2\,g^{-1}}$ and the density is $1.4 \times 10^{6}\,\mathrm{g\,m^{-3}}$. From this we obtain the saturation magnetization ($9.24\,\mathrm{kA\,m^{-1}}$), resulting in an α_p of $185\,\mathrm{kA^2\,N^{-1}}$. We focus on determining the force contribution of a single coil on a particle. We assume the particle to be a perfect sphere with a radius r_p. Combining (1) and (2) results in:

$$\mathbf{F} = \alpha_\mathrm{p} \frac{4}{3} \pi r_\mathrm{p}^3 \nabla(B^2) \tag{3}$$

In order to determine the drag force on the particle, we first determine the Reynolds number,

$$Re = \frac{2 \rho v r_\mathrm{p}}{\eta} \tag{4}$$

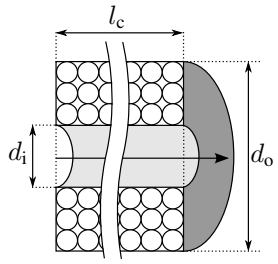

Fig. 4. Schematic of a coil used in the experimental setup. The arrow indicates the axial axis of the coil.

where v is the velocity of the particle, η dynamic viscosity (1 mPa s) and ρ the density of water (998.2 kg m^{-3}), both at room temperature. Assuming that v will not exceed 1 mm s^{-1}, we find a Reynolds number less than 0.1 for a particle with a diameter of 100 µm. We can therefore assume laminar flow conditions, and use the Stokes law for drag force F_d [2],

$$F_d = -6\pi\eta r_p v \tag{5}$$

The maximum velocity of a particle is reached when the drag force equals the magnetic force. In order to estimate the expected particle velocities, we combine (3) and (5). The maximum velocity of a paramagnetic particle (v_m) will be,

$$v_m = \frac{2}{9}\frac{\alpha_p r_p^2}{\eta}\nabla(B^2) \tag{6}$$

The above holds for $Re < 0.1$.

C. Coils

In order to generate the magnetic field needed to move the particles, we use four equally sized coils. Using the constraints given in Section II-A, we have chosen coils with an inner diameter d_i = 10 mm, an outer diameter d_o = 39 mm and a length of l_c = 30 mm. The coils have 1680 turns of 0.5 mm round enameled copper wire (magnet wire). A schematic view of the coil is shown in Fig. 4. The average self inductance and series resistance of the coils is measured to be ∼25 mH and ∼12 Ω, respectively. The inductance and resistance were measured at 1 kHz at room temperature using a Hameg MH8118 LCR meter (HAMEG Instruments GmbH, Mainhausen, Germany).

In order to verify whether the estimated coils will be sufficient to position a particle, we performed an analysis using a finite element method (FEM) simulation. The FEM model was created in Comsol Multiphysics® (COMSOL, Inc., Burlington, U.S.A). We modeled the coil as a thick hollow cylinder. The maximum current applied to the coils will be 0.8 A. The current density in the cylinder is assumed to correspond to a current of 0.8 A in the coil. Since we are interested in the gradient inside our reservoir, we assume the center of this reservoir is 20 mm from the coil. Fig. 5 shows the gradient of B^2 around the center of the reservoir in the axial direction of the coil. In this case the coil is located on the negative side of the X-axis. Fig. 5 shows that the gradient in the center of the container is ∼1.8 mT^2 m^{-1}. Using (6) for a 100 µm particle we predict a maximum velocity of 149 µm s^{-1} due to the force of one magnet.

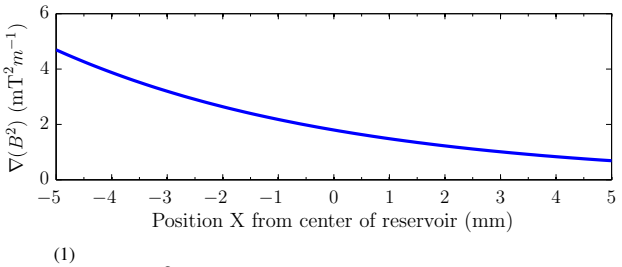

(1)

Fig. 5. Gradient of B^2 in the axial direction of the coil around the center of the reservoir for a current of 0.8 A.

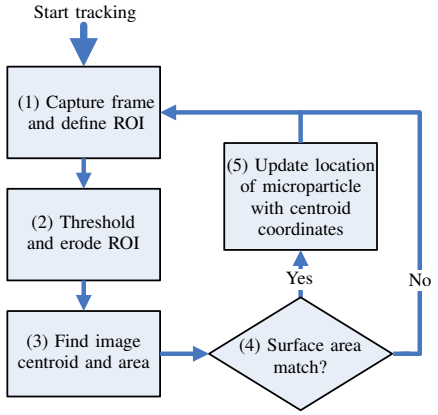

Fig. 6. Software flow with: (1) Frame capture and ROI definition (2) Adaptive thresholding and filtering (3) Centroid and area determination (4) Area checking (5) Updating the particle coordinates. The loop is run every 100 ms

D. Image-based particle tracking

Tracking of the particles is done by use of image feedback from the black and white camera mounted on the microscope. The images captured by the camera are imported to a computer (Microsoft Windows XP SP3) running software capable of image processing. The software is written in C using the open-source computer vision libraries *OpenCV* [16]. The particle detection algorithm captures a frame every 100 ms. It then locates the particle using the steps depicted in Fig. 6 and explained below:

- The program captures a frame and defines a Region Of Interest (ROI). The center of the ROI can either be selected by the user or it is the last known location of the particle.
- The gray-scale image within the ROI is converted to a binary (monochrome) image using an adaptive thresholding algorithm. The algorithm takes the mean pixel value and subtracts the standard deviation of the pixel values in the ROI to determine a good threshold value. The adaptive nature of the thresholding makes the algorithm less dependent on lighting conditions.
- The resulting binary image is filtered using three iterations of an erosion filter to remove unwanted noise (the assumption is made that the particle is the only large object in the ROI).
- The image moments for the filtered binary image are determined. From these image moments the centroid coordinates and the area of the image are determined.

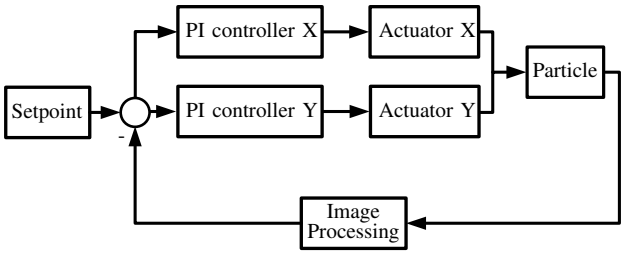

Fig. 7. Schematic diagram of the control loop. Two PI controllers are used to control the particle in both X and Y directions

- Finally, the calculated area is compared to the expected area of a particle. If the area is too large or too small to be a particle, it is assumed that no particle was detected and the particle coordinates are not updated. Thus, losing track of the particle. If the algorithm decides a particle was detected then the centroid coordinates become the new coordinates for the particle.

A limitation of the tracking algorithm is that it has a low immunity for errors that occur when multiple particles are inside the ROI. The algorithm assumes that there is only one particle in the image. If a second particle (or some other dark colored object) is in the ROI, the calculated centroid will be that of the combined particles. If the image with two particles does pass the area size test, the particle location is updated with incorrect coordinates. If the area size test fails, the tracker assumes it has lost the particle and the coordinates will no longer be updated. Since the preliminary experiments will be done in a controlled environment, most particle disturbances can be eliminated by careful preparation.

E. Magnetic control

In order to control the movement of the particle to a given setpoint, a PI controller was implemented for each axis. The controllers run in a closed loop with the tracking software depicted in Fig. 7. Both controllers use equivalent settings for the proportional and and integral gains. The tracking algorithm provides the PI controllers with the difference between the actual position and the desired position of the particle. The update rate of the control loop is $100\,\mathrm{ms}$, which is equal to the frame capturing rate of the particle tracking algorithm. Each axis is controlled independently and only one magnet is active per axis at the same time, depending on the direction in which the force should be applied to the particle. We have found no critical timing issues running the controllers at $10\,\mathrm{Hz}$.

F. System integration

The electromagnets are integrated into the setup that can be seen in Fig. 8. This setup allows the electromagnets to be positioned around the fluid reservoir. They are powered by Elmo 'Whistle' 1/60 servo controllers (Elmo Motion Control, Petach-Tikva, Israel) that are used as digitally controlled current sources. Each coil has its own dedicated controller to maximize flexibility of the system. The output current of these controllers is determined by the PI controllers. The computer uses an Arduino microcontroller board (http://www.arduino.cc) to interface with each of the four current sources. The power supplied to the current sources comes from a $48\,\mathrm{V}$, $5.2\,\mathrm{A}$ switched mode power supply unit.

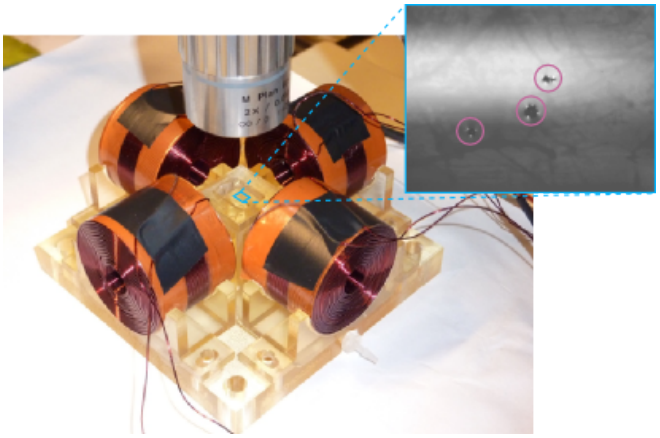

Fig. 8. Picture of the designed and assembled setup. Four coils fixed in a frame around a reservoir for liquids. The microscope objective is positioned above the reservoir. The image captured by the camera shows three particles.

III. RESULTS

In order to evaluate the positioning and tracking performance of the system, the following two experiments were conducted. First, an experiment to demonstrate the ability of the system to position the particle at a given setpoint. Second, an experiment to demonstrate the possibility to move the particle around a preset path of setpoints. For each experiment a single particle was selected. This particle had to be floating in the water-to-air boundary layer so it would not be affected by the surface friction at the bottom of the reservoir. The particle tracking algorithm performed adequately in locating the particles. Variations of contrast in the image did not cause the tracker to lose the particle. Several preliminary experiments were done with respect to positioning the particle. For each experiment, the gains were chosen such that the response of the system seemed suitable to perform the desired task. All resulting figures are based on the output provided by the tracking algorithm. Fig. 9(a) shows a step response of the system. The controller gains were set to $K_\mathrm{p} = 13$ and $K_\mathrm{i} = 0.5$. As can be seen in Fig. 9(b), there is a significant amount of overshoot in the particle trajectory. We argue this overshoot is mostly due to the integral action of the controller that needs time to recover and the movement of the fluid in which the particle resides. Changing the gains of the controller did reduce the overshoot on some occasions, however disturbances such as the flow of the fluid due to heat from the microscope light and air movement at the surface were compensated poorly.

From Fig. 9(a), we determine that the velocity of the particle was $182\,\mu\mathrm{m\,s^{-1}}$ in the X-direction and $148\,\mu\mathrm{m\,s^{-1}}$ in the Y-direction. This gives a total particle speed of $235\,\mu\mathrm{m\,s^{-1}}$. We estimate the size of the particle used in this experiment to be $\sim 100\,\mu\mathrm{m}$. Using (6) we find a theoretical maximum velocity of $149\,\mu\mathrm{m\,s^{-1}}$ in the center of the reservoir due to a single coil. We see that the velocity in the Y-direction

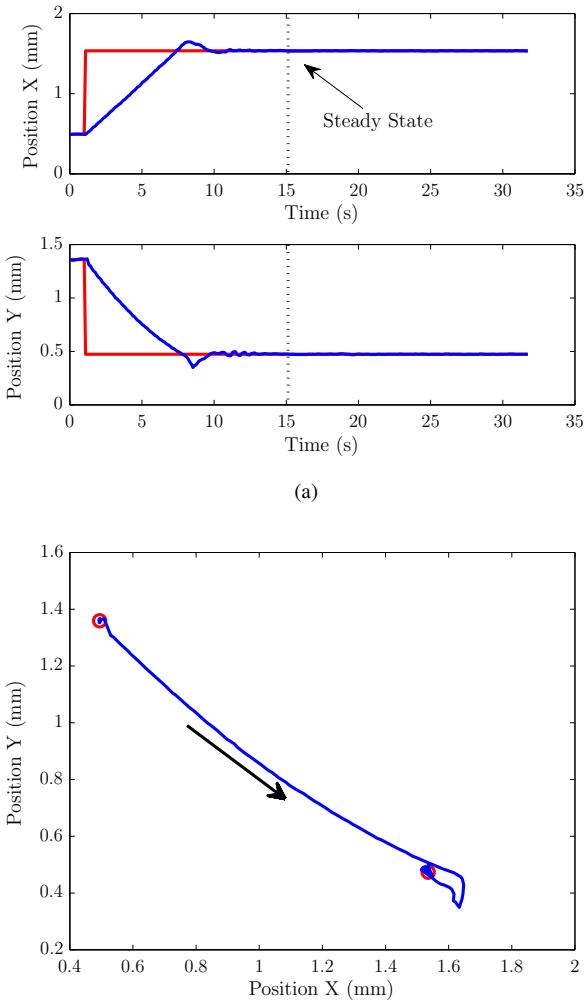

Fig. 9. Tracking performance to a single setpoint: (a) Each axis separately. (b) 2D trajectory of the combined axis. The red lines and circles represent the setpoints given to the controller. The arrow indicates the direction of movement.

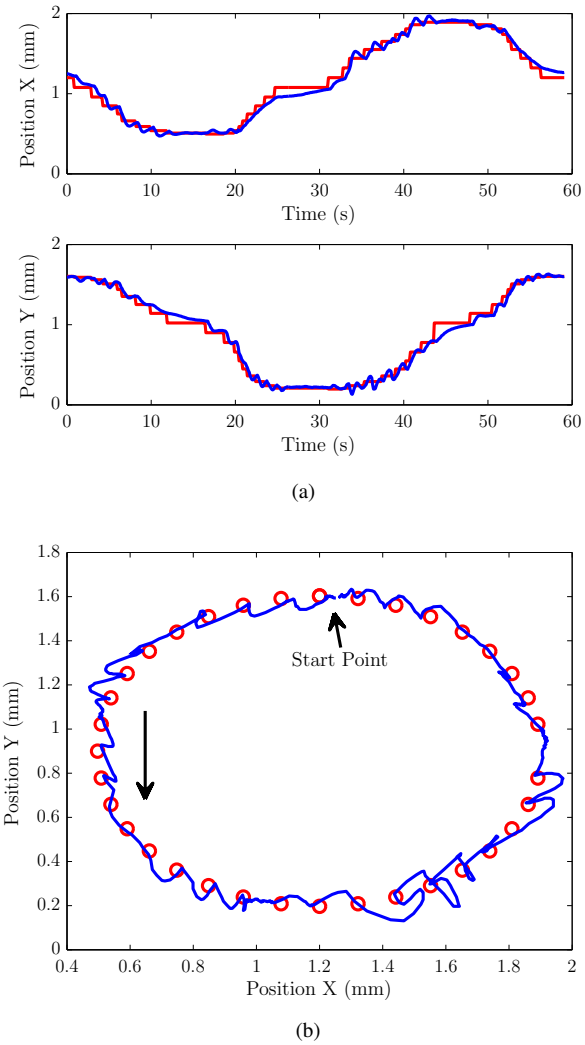

Fig. 10. Tracking performance of a circular path: (a) Each axis separately. (b) 2D trajectory of the combined axis. The red lines and circles represent the setpoints given to the controller. The arrow indicates the direction of movement. The controller gains were $K_\mathrm{p} = 3$ and $K_\mathrm{i} = 1.8$.

corresponds to the theoretical value quite well. The velocity in the X-direction however is significantly larger than expected. We attribute this difference to discrepancies between the ideal model and the experimental implementation. The particles are not completely submerged, which reduces their drag. Additionally, the magnetic field is not entirely uniform, resulting in coupling between forces along X and Y. Finally, the aforementioned flow of the liquid also influences the observed motion of the particle.

In order to determine the positioning accuracy we define the error as the difference between the actual and the desired position of the particle. Fig. 9(a) shows that the particle reached a steady state around the desired position after 15 s. The standard deviation of the error and the maximum error in steady-state were calculated from a set of 174 data points (Table I).

Figs. 10 and 11 show the results when a series of setpoints are given that describe a circular path and a figure-eight path, respectively. For these experiments a new setpoint is given when the particle is within 10 pixels ($\sim$23 µm) of the desired position. In the circular path, the average velocity of the particle was 83 µm s^{-1}. For the figure-eight path, the average velocity of the particle was 122 µm s^{-1}.

Most of the time it was not possible to use the same particle for multiple experiments. In our setup, the particles dried out and disintegrated after some time. New particles were taken for each experiment. We found, as expected from (6), that the size of the particle has a significant influence on the particles velocity. Therefore, for all experiments done, we have tried to manually select particles, that appeared have an equal size.

TABLE I

TABLE SHOWING THE STANDARD DEVIATION AND THE MAXIMUM VALUE OF THE ERROR IN STEAD-STATE (> 15 s)

Axis	Standard Deviation (µm)	Maximum Error (µm)
X	1.8	4.7
Y	2.0	7.0

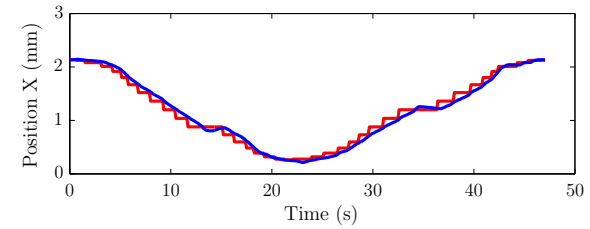

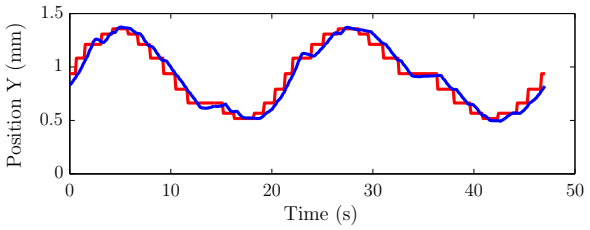

(a)

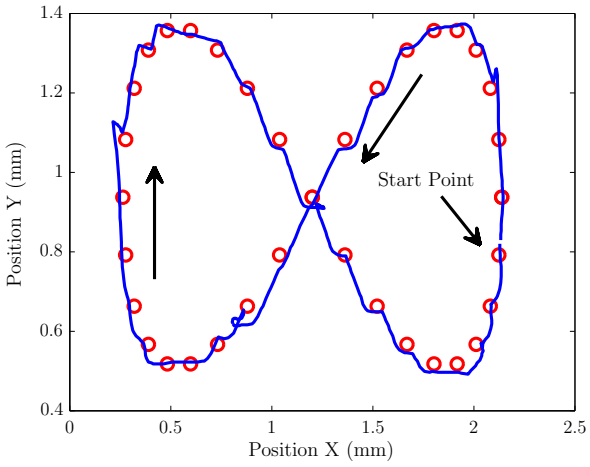

(b)

Fig. 11. Tracking performance of a figure-eight path: (a) Each axis separately. (b) 2D trajectory of the combined axis. The red lines and circles represent the setpoints given to the controller. The arrows indicate the direction of movement. The controller gains were K_p = 15.5 and K_i = 1.2.

IV. CONCLUSIONS AND FUTURE WORK

We have shown that it is possible to control the position of paramagnetic microparticles suspended in water. This was accomplished using four electromagnets in a closed control loop with image-based feedback. We have demonstrated that with a fairly basic setup and a simple control algorithm that we were able to position a particle, with a average diameter of 100 µm, within 8.4 µm of a desired position. The particle was observed to be traveling with a velocity of 235 µm s^{-1}. We have also demonstrated that we were able to steer the particle along a circular and figure-eight path.

The experimental setup and the preliminary results are the basis for future work to control self-propelled microrobots. To improve the positioning accuracy of the microrobot we aim to expand the controller to a model-based approach. The microrobots will be made out of platinum and cobalt, and will be placed in a reservoir that contains a solution of hydrogen peroxide (H_2O_2). The propulsion will come from the catalytic reaction that occurs between platinum and H_2O_2. Propulsion forces from this reaction can, for instance come in the form of oxygen bubbles that exert a force upon the microrobot [12]. When a combination of gold and platinum is used, propulsion can come from a process called self-electrophoresis [17]. When the microrobot will have its own propulsion, only control of the orientation of the robot is required. In this case, the magnetic fields will be utilized to exert a torque on the microrobot rather then a force. This can be achieved by integrating a magnetic strip inside the microrobot and exert a torque (τ) on it according to $\tau = \mathbf{m} \times \mathbf{B}$. One of the advantages of using self-propelled robots over passive robots is the fact that the amount of magnetic energy needed to rotate an object is significantly less than to actually displace it. As a result, the size and cost of the required magnets will reduce considerably.

Acknowledgements - The authors would like to thank Gerben te Riet o/g Scholten, Martin Siekman and Thijs Bolhuis (University of Twente) for their assistance and advice regarding the design of the setup.

REFERENCES

[1] Menciassi *et al.*, "Microrobotics for future gastrointestinal endoscopy," *Minimally Invasive Therapy Allied Technologies*, vol. 16, no. 2, pp. 91–100, 2007.
[2] Abbott *et al.*, "Robotics in the small, part I: Microrobotics," *IEEE Robotics & Automation Magazine*, vol. 14, no. 2, pp. 92–103, 2007.
[3] Abbott *et al.*, "How should microrobots swim?," *Int'l. J. Robotics Research*, vol. 28, no. 11-12, pp. 1434–1447, 2007.
[4] Kummer *et al.*, "Octomag: an electromagnetic system for 5-dof wireless manipulation," in *Proc. IEEE Int'l. Conf. Robotics and Automation*, (Anchorage, Alaska), pp. 1610–1616, May 2010.
[5] Choi *et al.*, "Two-dimensional actuation of a microrobot with a stationary two-pair coil system," *Smart Materials and Structures*, vol. 18, no. 5, 2009.
[6] Yesin *et al.*, "Modeling and control of untethered biomicrorobots in a fluidic environment using electromagnetic fields," *Int'l. J. Robotics Research*, vol. 25, pp. 527–536, 2006.
[7] Mathieu *et al.*, "Method of propulsion of a ferromagnetic core in the cardiovascular system through magnetic gradients generated by an mri system," *IEEE Trans Biomed Eng*, vol. 53, no. 2, pp. 292–299, 2006.
[8] J.-B. Mathieu and S. Martel, "Steering of aggregating magnetic microparticles using propulsion gradients coils in an MRI scanner," *Magnetic Resonance Medicine*, vol. 63, no. 5, pp. 1336–1345, 2010.
[9] Fountain *et al.*, "Wireless control of magnetic helical microrobots using a rotating-permanent-magnet manipulator," in *Proc. IEEE Int'l. Conf. Robotics and Automation*, (Anchorage, Alaska), pp. 576–581, May 2010.
[10] Peyer *et al.*, "Non-ideal swimming of artificial bacterial flagella near a surface," in *Proc. IEEE Int'l. Conf. Robotics and Automation*, (Anchorage, Alaska), pp. 96–101, May 2010.
[11] S. Martel and M. Mohammadi, "Using a swarm of self-propelled natural microrobots in the form of flagellated bacteria to perform complex micro-assembly tasks," in *Proc. IEEE Int'l. Conf. Robotics and Automation*, (Anchorage, Alaska), pp. 500–505, May 2010.
[12] Ismagilov *et al.*, "Autonomous movement and self-assembly," *Angewandte Chemie*, vol. 114, no. 4, pp. 674–676, 2002.
[13] Mirkovic *et al.*, "Nanolocomotion - catalytic nanomotors and nanorotors," *Small*, vol. 6, pp. 159–167, January 2010.
[14] Sundararajan *et al.*, "Catalytic motors for transport of colloidal cargo," *Nano Letters*, vol. 8, no. 5, pp. 1271–1276, 2008.
[15] Solovev *et al.*, "Catalytic microtubular jet engines self-propelled by accumulated gas bubbles.," *Small*, vol. 5, no. 14, pp. 1688–92, 2009.
[16] G. Bradski and A. Kaehler, *Learning OpenCV: computer vision with the OpenCV library*. O'Reilly Media, first ed., 2008.
[17] Paxton *et al.*, "Motility of catalytic nanoparticles through self-generated forces," *Chemistry A European Journal*, vol. 11, no. 22, pp. 6462–6470, 2005.